Optics Communications 282 (2009) 661–665

Contents lists available at ScienceDirect

Optics Communications

journal homepage: www.elsevier.com/locate/optcom

Optical response of small-diameter semiconducting carbon nanotubes under exciton–surface-plasmon coupling

I.V. Bondarev [a,*], K. Tatur [b], L.M. Woods [b]

[a] Physics Department, North Carolina Central University, 1801 Fayetteville Str., Durham, NC 27707, USA
[b] Physics Department, University of South Florida, 4202 E.Fowler Ave., Tampa, FL 33620, USA

ARTICLE INFO

Article history:
Received 4 June 2008
Received in revised form 15 October 2008
Accepted 30 October 2008

PACS:
78.40.Ri
73.22.−f
73.63.Fg
78.67.Ch

ABSTRACT

We analyze the optical response of small-diameter ($\lesssim$1 nm) semiconducting carbon nanotubes under the exciton–surface-plasmon coupling. Calculated optical absorption lineshapes exhibit the significant line (Rabi) splitting ~0.1–0.3 eV as the exciton energy is tuned to the nearest interband surface plasmon resonance of the nanotube so that the mixed strongly coupled surface plasmon–exciton excitations are formed. We discuss possible ways to bring the exciton in resonance with the surface plasmon. The exciton–plasmon Rabi splitting effect we predict here for an individual carbon nanotube is close in its magnitude to that previously reported for hybrid plasmonic nanostructures artificially fabricated of organic semiconductors deposited on metallic films. We believe this effect may be used for the development of carbon nanotube based tunable optoelectronic device applications in areas such as nanophotonics and cavity quantum electrodynamics.

Single-walled carbon nanotubes (CNs) are quasi-one-dimensional (1D) cylindrical wires consisting of graphene sheets rolled-up into cylinders with diameters ~1–10 nm and lengths ~1–10^4 μm [1–3]. CNs are shown to be useful for miniaturized electronic, electromechanical, chemical and scanning probe devices and as materials for macroscopic composites [4]. The area of their potential applications has been recently expanded towards nanophotonics and optoelectronics [5,6] after the experimental demonstration of controllable single-atom incapsulation into single-walled CNs [7,8].

For pristine (undoped) single-walled CNs, the numerical calculations predicting large exciton binding energies (~0.3–0.6 eV) in semiconducting CNs [9–11] and even in some small-diameter (~0.5 nm) metallic CNs [12], followed by the results of various measurements of the excitonic photoluminescence [13–16], have become available. These works, together with other reports investigating the role of effects such as intrinsic defects [15], exciton–phonon interactions [16–19], external magnetic and electric fields [20,21], reveal the variety and complexity of the intrinsic optical properties of carbon nanotubes.

One of us have reported earlier the interactions between excitonic states and surface electromagnetic (EM) fluctuations to result in the strong exciton–surface-plasmon coupling in small-diameter ($\lesssim$1 nm) semiconducting single-walled CNs [22]. The reason is, due to the nanotube quasi-one-dimensionality, the exciton transition dipole moment matrix element and the quasi-momentum vector are directed predominantly along the CN axis (the longitudinal exciton). This prevents the exciton from the electric dipole coupling to the transversely polarized surface EM modes of the nanotube as they propagate predominantly along the CN axis with their electric vectors orthogonal to the propagation direction. The longitudinally polarized surface EM modes are generated by the electronic Coulomb potential (see, e.g., Ref. [23]), and therefore represent the CN surface plasmon excitations. These have their electric vectors directed along the propagation direction. They do couple to the longitudinal excitons on the CN surface [22]. Such modes were observed in Ref. [24] to occur in the same energy range of ~1 eV where the exciton excitation energies are located in small-diameter ($\lesssim$1 nm) semiconducting CNs [25,26]. They are the weakly-dispersive interband plasmon modes [27] similar to the intersubband plasmon modes in quantum wells [28].

Here we analyze the optical response of small-diameter semiconducting CNs under the strong exciton–surface-plasmon coupling. The calculated optical absorption lineshapes of the (11,0) and (10,0) CNs exhibit the significant line (Rabi) splitting effect ~0.1 eV as the exciton energy is tuned to the nearest interband surface plasmon resonance of the nanotube. This result is particularly interesting since it reveals the fundamental EM phenomenon – the strong exciton–plasmon coupling – in an *individual* quasi-one-dimensional (1D) nanostructure, a carbon nanotube, as opposed to various artificially fabricated *hybrid* plasmonic nanostructures, such as dye molecules in organic polymers deposited on metallic films [29], semiconductor quantum dots coupled to metal-

* Corresponding author.
E-mail address: ibondarev@nccu.edu (I.V. Bondarev).

0030-4018/$ - see front matter © 2008 Elsevier B.V. All rights reserved.
doi:10.1016/j.optcom.2008.10.074

lic nanoparticles [30], or nanowires [31], where semiconductor material carries the exciton and metal carries the plasmon.

The energy $\hbar\omega_\mu(\mathbf{k})$ of the coupled exciton–surface-plasmon excitation of branch μ $(=1,2)$ is given by the integral dispersion relation [22], which is written in the dimensionless form as follows:

$$x_\mu^2 - \varepsilon_f^2 - \frac{\varepsilon_f}{2\pi}\int_0^\infty dx \frac{x\overline{\Gamma}_0^f(x)\rho(x)}{x_\mu^2 - x^2} = 0. \tag{1}$$

Here,

$$x = \frac{\hbar\omega}{2\gamma_0}, \quad x_\mu = \frac{\hbar\omega_\mu(\mathbf{k})}{2\gamma_0}, \quad \varepsilon_f = \frac{E_f(\mathbf{k})}{2\gamma_0} \tag{2}$$

with $\gamma_0 = 2.7$ eV being the carbon nearest neighbor overlap integral entering the CN surface axial conductivity σ_{zz} (the CN axis is assigned to be the z-axis of the cylindrical coordinate system we use, and we neglect much smaller azimuthal conductivity component $\sigma_{\varphi\varphi}$ in our model). The total energy $E_f(\mathbf{k})$ of the f-internal-state exciton with the quasi-momentum $\mathbf{k} = \{k_\varphi, k_z\}$, where k_z is continuous and k_φ is quantized due to the transverse confinement effect, is given by

$$E_f(\mathbf{k}) = E_{exc}^{(f)}(k_\varphi) + \frac{\hbar^2 k_z^2}{2M_{ex}} \tag{3}$$

with the first term representing the excitation energy, $E_{exc}^{(f)}(k_\varphi) = E_g(k_\varphi) + E_b^{(f)}$, of the f-internal-state exciton with the (negative) binding energy $E_b^{(f)}$, created via the interband transition with the band gap $E_g(k_\varphi) = \varepsilon_e(k_\varphi) + \varepsilon_h(k_\varphi)$, where $\varepsilon_{e,h}$ are transversely quantized azimuthal electron–hole subbands (see the schematic in Fig. 1). The second term represents the kinetic energy of the translational longitudinal movement of the exciton with the effective mass $M_{ex} = m_e + m_h$, where m_e and m_h are the electron and hole effective masses, respectively. The function

$$\overline{\Gamma}_0^f(x) = \frac{4|d_z^f|^2 x^3}{3\hbar c^3}\left(\frac{2\gamma_0}{\hbar}\right)^2 \tag{4}$$

represents the (dimensionless) exciton spontaneous decay rate. Here, c is the speed of light and $d_z^f = \sum_{\mathbf{n}}\langle 0|(\hat{\mathbf{d}}_{\mathbf{n}})_z|f\rangle$ (summation over carbon atoms) is the longitudinal exciton transition dipole moment matrix element. The function

$$\rho(x) = \frac{3S_0}{4\pi\alpha R_{CN}^2}\,\mathrm{Re}\frac{1}{\bar{\sigma}_{zz}(x)} \tag{5}$$

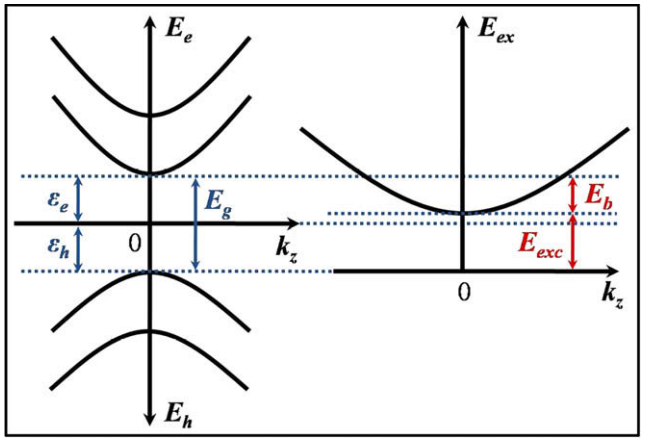

Fig. 1. Schematic of the transversely quantized azimuthal electron–hole subbands (*left*), and the first-interband ground-internal-state exciton energy (*right*) in a small-diameter semiconducting carbon nanotube. See text for notations.

stands for the surface plasmon density of states (DOS) which is responsible for the exciton decay rate variation due to the coupling to plasmon modes. Here, $S_0 = (3\sqrt{3}/4)b^2$ with $b = 1.42$ Å being the carbon–carbon interatomic distance, $\alpha = e^2/\hbar c = 1/137$ is the fine-structure constant, R_{CN} is the nanotube radius, and $\bar{\sigma}_{zz} = 2\pi\hbar\sigma_{zz}/e^2$ is the dimensionless CN surface axial conductivity per unit length.

Note that the conductivity factor in Eq. (5) equals

$$\mathrm{Re}\frac{1}{\bar{\sigma}_{zz}(x)} = -\frac{4\alpha c}{R_{CN}}\left(\frac{\hbar}{2\gamma_0 x}\right)\mathrm{Im}\frac{1}{\epsilon_{zz}(x) - 1} \tag{6}$$

in view of Eq. (2) and the formula $\sigma_{zz} = -i\omega(\epsilon_{zz} - 1)/4\pi S\rho_T$ representing the Drude relation for CNs, where ϵ_{zz} is the longitudinal dielectric function, S and ρ_T are the surface area of the tubule and the number of tubules per unit volume, respectively [32–35]. This relates very closely the surface plasmon DOS function Eq. (5) to the loss function $-\mathrm{Im}(1/\epsilon)$ measured in electron energy loss spectroscopy (EELS) experiments to determine the properties of collective electronic excitations in solids [24].

Fig. 2 shows the low-energy behaviors of the functions $\bar{\sigma}_{zz}(x)$ and $\mathrm{Re}[1/\bar{\sigma}_{zz}(x)]$ for the (11,0) and (10,0) CNs ($R_{CN} = 0.43$ nm and 0.39 nm, respectively) we study here. We obtained them numerically as follows. First, we adapt the nearest-neighbor non-orthogonal tight-binding approach [36] to determine the realistic band structure of each CN. Then, the room-temperature longitudinal dielectric functions ϵ_{zz} are calculated within the random-phase approximation [37,38], which are then converted into the conductivities $\bar{\sigma}_{zz}$ by means of the Drude relation. Electronic dissipation processes are included in our calculations within the relaxation-time approximation (electron scattering length of $130R_{CN}$ was used [18]). We did not include excitonic many-electron correlations, however, as they mostly affect the real conductivity $\mathrm{Re}(\bar{\sigma}_{zz})$ which is responsible for the CN optical absorption [10,12,39], whereas we are interested here in $\mathrm{Re}(1/\bar{\sigma}_{zz})$ representing the surface plasmon DOS according to Eq. (5). This function is only non-zero when the two conditions, $\mathrm{Im}[\bar{\sigma}_{zz}(x)] = 0$ and $\mathrm{Re}[\bar{\sigma}_{zz}(x)] \to 0$, are fulfilled simultaneously [27,28,37]. These result in the peak structure of the function $\mathrm{Re}(1/\bar{\sigma}_{zz})$ as is seen in Fig. 2. It is also seen from the comparison of Fig. 2b with Fig. 2a that the peaks broaden as the CN diameter decreases. This is consistent with the stronger hybridization effects in smaller-diameter CNs [40].

Left panels in Fig. 3a and b show the lowest-energy plasmon DOS resonances calculated for the (11,0) and (10,0) CNs as given by the function $\rho(x)$ in Eq. (5). The corresponding fragments of the functions $\mathrm{Re}[\bar{\sigma}_{zz}(x)]$ and $\mathrm{Im}[\bar{\sigma}_{zz}(x)]$ are also shown there. In all graphs the lower dimensionless energy limits are set up to be equal to the lowest bright exciton excitation energy [$E_{exc} = 1.21$ eV ($x = 0.224$) and 1.00 eV ($x = 0.185$) for the (11,0) and (10,0) CN, respectively, as reported in Ref. [25] by directly solving the Bethe–Salpeter equation]. Peaks in $\rho(x)$ are seen to coincide in energy with zeros of $\mathrm{Im}[\bar{\sigma}_{zz}(x)]$ {or zeros of $\mathrm{Re}[\epsilon_{zz}(x)]$}, clearly indicating the plasmonic nature of the CN surface excitations under consideration [27,41]. They describe the surface plasmon modes associated with the transversely quantized interband electronic transitions in CNs [27]. As is seen in Fig. 3 (and in Fig. 2), the interband plasmon excitations occur in CNs slightly above the first bright exciton excitation energy [39], which is a unique feature of the complex dielectric response function – the consequence of the general Kramers–Krönig relation [42].

We further take advantage of the sharp peak structure of $\rho(x)$ and solve the dispersion Eq. (1) for x_μ analytically using the Lorentzian approximation

$$\rho(x) \approx \frac{\rho(x_p)\Delta x_p^2}{(x - x_p)^2 + \Delta x_p^2}. \tag{7}$$

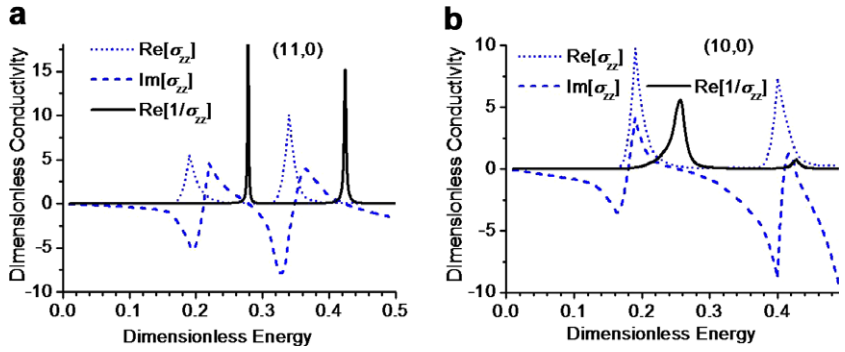

Fig. 2. (a) and (b) Calculated (see text) dimensionless axial surface conductivities for the (11,0) and (10,0) nanotubes. Dimensionless energy is defined as $[Energy]/2\gamma_0$, according to Eq. (2).

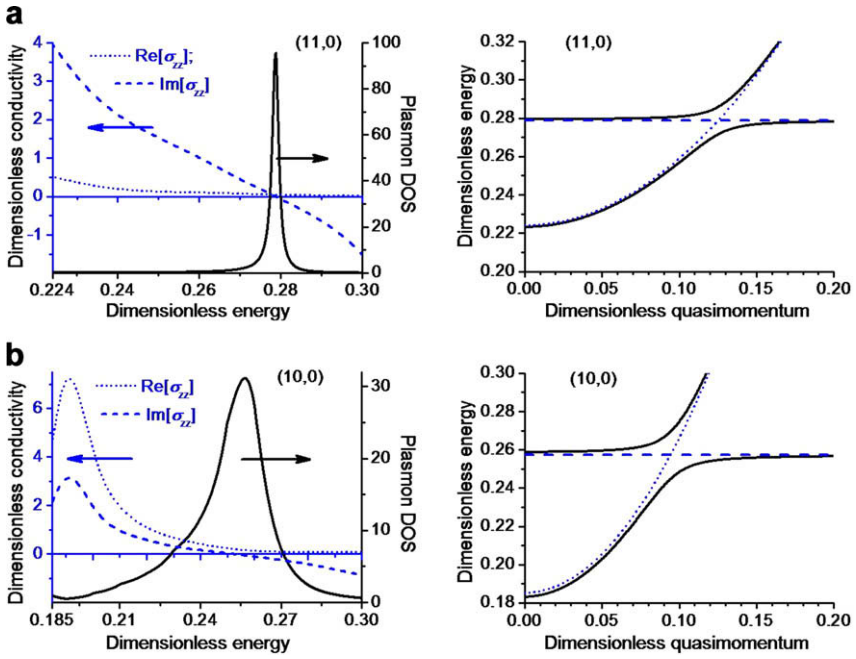

Fig. 3. (a) and (b) Surface plasmon DOS and conductivities (left panels), and lowest bright exciton dispersion when coupled to plasmons (right panels) in the (11,0) and (10,0) CN, respectively. Dimensionless energy is defined as $[Energy]/2\gamma_0$, according to Eq. (2). See text for dimensionless quasi-momentum.

Here, x_p and Δx_p are, respectively, the position and the half-width-at-half-maximum of the plasmon resonance closest to the lowest bright exciton excitation energy in the same nanotube (as shown in the left panels of Fig. 3). The integral in Eq. (1) then simplifies to the form

$$\frac{1}{2\pi}\int_0^\infty dx\frac{x\overline{\Gamma}_0^f(x)\rho(x)}{x_\mu^2-x^2}\approx\frac{F(x_p)\Delta x_p^2}{x_\mu^2-x_p^2}\int_0^\infty\frac{dx}{(x-x_p)^2+\Delta x_p^2}=\frac{F(x_p)\Delta x_p}{x_\mu^2-x_p^2}\left[\arctan\left(\frac{x_p}{\Delta x_p}\right)+\frac{\pi}{2}\right] \quad (8)$$

with $F(x_p)=x_p\overline{\Gamma}_0^f(x_p)\rho(x_p)/2\pi$. This expression is valid for all x_μ apart from those located in the narrow interval $(x_p-\Delta x_p, x_p+\Delta x_p)$ in the vicinity of the plasmon resonance, provided that the resonance is sharp enough. Then, the dispersion equation becomes the biquadratic equation for x_μ with the following two positive solutions (the dispersion curves) of interest to us:

$$x_{1,2}=\sqrt{\frac{\varepsilon_f^2+x_p^2}{2}\pm\frac{1}{2}\sqrt{(\varepsilon_f^2-x_p^2)^2+F_p\varepsilon_f}}. \quad (9)$$

Here, $F_p=4F(x_p)\Delta x_p(\pi-\Delta x_p/x_p)$, and the arctan-function of Eq. (8) is expanded into series to linear terms in $\Delta x_p/x_p\ll 1$.

The dispersion curves Eq. (9) are shown in the right panels in Fig. 3a and b as functions of the dimensionless longitudinal quasi-momentum. In these calculations, we estimated the interband transition matrix element in $\overline{\Gamma}_0^f(x_p)$ [Eq. (4)] from the equation $|d_z^f|^2=3\hbar\lambda^3/4\tau_{ex}^{rad}$ according to Hanamura's general theory of the exciton radiative decay in spatially confined systems [43], where τ_{ex}^{rad} is the exciton intrinsic radiative lifetime, and $\lambda=2\pi c\hbar/E$ with E being the exciton total energy given in our case by Eq. (3). For zigzag-type CNs we here consider, the first Brillouin zone of the longitudinal quasi-momentum is given by $-2\pi\hbar/3b\leqslant\hbar k_z\leqslant 2\pi\hbar/3b$ [1,2]. The total energy of the ground-internal-state exciton can then be written as $E=E_{exc}+(2\pi\hbar/3b)^2t^2/2M_{ex}$ with $-1\leqslant t\leqslant 1$ representing the dimensionless longitudinal quasi-momentum. In our calculations we used the lowest bright exciton parameters $E_{exc}=1.21$ eV and 1.00 eV, $\tau_{ex}^{rad}=14.3$ ps and 19.1 ps, $M_{ex}=0.44m_0$ and $0.19m_0$ (m_0 is the free-electron mass) for the (11,0) CN and (10,0) CN, respectively, as reported in Ref. [25] by directly solving the Bethe–Salpeter equation.

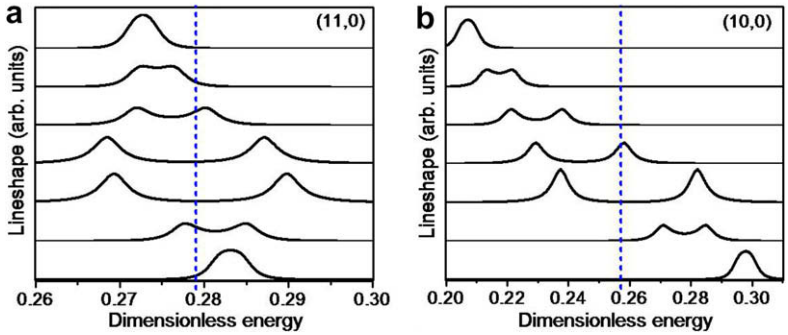

Fig. 4. (a) and (b) Exciton absorption lineshapes as the exciton energies are tuned to the nearest plasmon resonance energies (vertical dashed lines here; see Fig. 3, left panels) in the (11,0) and (10,0) CN, respectively. Dimensionless energy is defined as $[Energy]/2\gamma_0$, according to Eq. (2).

Both graphs in the right panels in Fig. 3 are seen to demonstrate a clear anticrossing behavior with the (Rabi) energy splitting ~0.1 eV. This indicates the formation of the strongly coupled surface plasmon–exciton excitations in the nanotubes under consideration. It is important to realize that here we deal with the strong exciton–plasmon interaction supported by an individual quasi-1D nanostructure – a single-walled (small-diameter) semiconducting carbon nanotube, as opposed to the artificially fabricated metal–semiconductor nanostructures studied previously [29–31] where the metallic component normally carries the plasmon and the semiconducting one carries the exciton. It is also important that the effect comes not only from the height but also from the width of the plasmon resonance as is seen from the definition of the F_p factor in Eq. (9). In other words, as long as the plasmon resonance is sharp enough (which is always the case for interband plasmons), so that the Lorentzian approximation Eq. (7) applies, the effect is determined by the area under the plasmon peak in the DOS function Eq. (5) rather then by the peak height as one would expect.

We are now in a position to derive the exciton absorption lineshape function. To do that, we follow the optical absorption lineshape theory that one of us developed recently for atomically doped CNs [5]. In doing so, we take into account the exciton–phonon scattering in the relaxation time approximation. The (dimensionless) exciton absorption lineshape function $I(x)$ in the vicinity of the plasmon resonance is then of the form

$$I(x) = \frac{I_0(x_p)[(x-\varepsilon_f)^2 + \Delta x_p^2]}{[(x-\varepsilon_f)^2 - X_f^2/4]^2 + (x-\varepsilon_f)^2(\Delta x_p^2 + \Delta\varepsilon_f^2)}, \qquad (10)$$

where $I_0(x_p) = \overline{\Gamma}_0^f(x_p)\rho(x_p)/2\pi$, $X_f = \sqrt{4\pi\Delta x_p I_0(x_p)}$, and $\Delta\varepsilon_f = \hbar/2\gamma_0\tau_{ph}$ ($< \Delta x_p$) is the exciton energy broadening due to the phonon scattering with the relaxation time τ_{ph}.

The calculated exciton absorption lineshapes for the CNs under consideration are shown in Fig. 4a and b as the exciton energies are tuned to the nearest plasmon resonances. We used $\tau_{ph} = 30$ fs as reported in Ref. [17]. The line (Rabi) splitting effect is seen to be ~0.1–0.3 eV, indicating the strong exciton–plasmon coupling with the formation of the mixed surface plasmon–exciton excitations. The splitting is larger in the smaller diameter nanotubes, and is not masked by the exciton–phonon scattering.

Thus, we have shown the strong exciton–surface-plasmon coupling effect with the characteristic exciton absorption line (Rabi) splitting ~0.1–0.3 eV in small-diameter ($\lesssim$1 nm) semiconducting CNs. This is almost as large as the typical exciton binding energies in such CNs (~0.3–0.8 eV [9–11,14]), and of the same order of magnitude as the exciton–plasmon Rabi splitting in organic semiconductors (~180 meV [29]). Also, this is much larger than the exciton–polariton Rabi splitting in semiconductor microcavities (~140–400 μeV [44–46]), or the exciton–plasmon Rabi splitting in hybrid semiconductor–metal nanoparticle molecules [30]. However, the formation of the strongly coupled exciton–plasmon states is only possible if the exciton total energy is in resonance with the energy of an interband surface plasmon mode. The exciton energy might be tuned to the nearest plasmon resonance in ways used for the excitons in semiconductor quantum microcavities – thermally (by elevating sample temperature) [44–46], and/or electrostatically [47–50] (via the quantum confined Stark effect with an external electrostatic field applied perpendicular to the CN axis). The two possibilities influence the different degrees of freedom of the quasi-1D exciton – the (longitudinal) kinetic energy and the excitation energy, respectively [see Eq. (3)]. In the latter case, plasmon and exciton resonances both shift to the red due to the decrease in E_g as the field increases [48]. However, the exciton shift is approximately twice as less due to the decrease in $|E_b|$ (see Ref. [48]), which is enough for the resonance to occur in view of the large $|E_b|$ contribution ~ $0.5E_{exc}$ in small-diameter CNs [9–11,14]. This effect may be used for the development of CN based tunable optoelectronic device applications in areas such as nanophotonics and cavity quantum electrodynamics.

Acknowledgements

The work is supported by NSF (Grant Nos. ECS-0631347 and HRD-0833184). K.T. and L.M.W. are supported by DOE (Grant No. DE-FG02-06ER46297). I.V.B. acknowledges fruitful discussions with Alexander Govorov and Jonathan Finley.

References

[1] R. Saito, G. Dresselhaus, M.S. Dresselhaus, Science of Fullerens and Carbon Nanotubes, Imperial College Press, London, 1998.
[2] H. Dai, Surf. Sci. 500 (2002) 218.
[3] L.X. Zheng, M.J. O'Connell, S.K. Doorn, X.Z. Liao, Y.H. Zhao, E.A. Akhadov, M.A. Hoffbauer, B.J. Roop, Q.X. Jia, R.C. Dye, D.E. Peterson, S.M. Huang, J. Liu, Y.T. Zhu, Nat. Mater. 3 (2004) 673.
[4] R.H. Baughman, A.A. Zakhidov, W.A. de Heer, Science 297 (2002) 787.
[5] I.V. Bondarev, B. Vlahovic, Phys. Rev. B 74 (2006) 073401.
[6] I.V. Bondarev, B. Vlahovic, Phys. Rev. B 75 (2007) 033402.
[7] G.-H. Jeong, A.A. Farajian, R. Hatakeyama, T. Hirata, T. Yaguchi, K. Tohji, H. Mizuseki, Y. Kawazoe, Phys. Rev. B 68 (2003) 075410.
[8] G.-H. Jeong, A.A. Farajian, T. Hirata, R. Hatakeyama, K. Tohji, T.M. Briere, H. Mizuseki, Y. Kawazoe, Thin Solid Films 435 (2003) 307.
[9] T. Pedersen, Phys. Rev. B 67 (2003) 073401.
[10] T. Pedersen, Carbon 42 (2004) 1007.
[11] R.B. Capaz, C.D. Spataru, S. Ismail-Beigi, S.G. Louie, Phys. Rev. B 74 (2006) 121401. R.
[12] C.D. Spataru, S. Ismail-Beigi, L.X. Benedict, S.G. Louie, Phys. Rev. Lett. 92 (2004) 077402.
[13] F. Wang, G. Dukovic, L.E. Brus, T.F. Heinz, Phys. Rev. Lett. 92 (2004) 177401.
[14] F. Wang, G. Dukovic, L.E. Brus, T.F. Heinz, Science 308 (2005) 838.
[15] A. Hagen, M. Steiner, M.B. Raschke, C. Lienau, T. Hertel, H. Qian, A.J. Meixner, A. Hartschuh, Phys. Rev. Lett. 95 (2005) 197401.
[16] F. Plentz, H.B. Ribeiro, A. Jorio, M.S. Strano, M.A. Pimenta, Phys. Rev. Lett. 95 (2005) 247401.

[17] V. Perebeinos, J. Tersoff, Ph. Avouris, Phys. Rev. Lett. 94 (2005) 027402.
[18] M. Lazzeri, S. Piscanec, F. Mauri, A.C. Ferrari, J. Robertson, Phys. Rev. Lett. 95 (2005) 236802.
[19] S. Piscanec, M. Lazzeri, J. Robertson, A. Ferrari, F. Mauri, Phys. Rev. B 75 (2007) 035427.
[20] S. Zaric, G.N. Ostojic, J. Shaver, J. Kono, O. Portugall, P.H. Frings, G.L.J.A. Rikken, M. Furis, S.A. Crooker, X. Wei, V.C. Moore, R.H. Hauge, R.E. Smalley, Phys. Rev. Lett. 96 (2006) 016406.
[21] V. Perebeinos, Ph. Avouris, Nano Lett. 7 (2007) 609.
[22] I.V. Bondarev, H. Qasmi, Physica E 40 (2008) 2365.
[23] L.D. Landau, E.M. Lifshits, The Classical Theory of Fields, Pergamon, New York, 1975.
[24] T. Pichler, M. Knupfer, M.S. Golden, J. Fink, A. Rinzler, R.E. Smalley, Phys. Rev. Lett. 80 (1998) 4729.
[25] C.D. Spataru, S. Ismail-Beigi, R.B. Capaz, S.G. Louie, Phys. Rev. Lett. 95 (2005) 247402.
[26] Y.-Z. Ma, C.D. Spataru, L. Valkunas, S.G. Louie, G.R. Fleming, Phys. Rev. B 74 (2006) 085402.
[27] K. Kempa, P.R. Chura, in: L. Liz-Marzan, M. Giersig (Eds.), Special edition of the Kluwer Academic Press Journal, 2002.
[28] K. Kempa, D. Broido, C. Beckwith, J. Cen, Phys. Rev. B 40 (1989) 8385.
[29] J. Bellessa, C. Bonnand, J.C. Plenet, J. Mugnier, Phys. Rev. Lett. 93 (2004) 036404.
[30] W. Zhang, A.O. Govorov, G.W. Bryant, Phys. Rev. Lett. 97 (2006) 146804.
[31] Y. Fedutik, V.V. Temnov, O. Schöps, U. Woggon, M.V. Artemyev, Phys. Rev. Lett. 99 (2007) 136802.
[32] I.V. Bondarev, Ph. Lambin, Phys. Rev. B 70 (2004) 035407;
I.V. Bondarev, Ph. Lambin, Phys. Lett. A 328 (2004) 235.
[33] I.V. Bondarev, Ph. Lambin, Phys. Rev. B 72 (2005) 035451;
I.V. Bondarev, Ph. Lambin, Solid State Commun. 132 (2004) 203.
[34] I.V. Bondarev, Ph. Lambin, in: Trends in Nanotubes Research, Nova Science, NY, 2006, pp. 139–183 (Chapter 6).
[35] S. Tasaki, K. Maekawa, T. Yamabe, Phys. Rev. B 57 (1998) 9301.
[36] V.N. Popov, L. Henrard, Phys. Rev. B 70 (2004) 115407.
[37] M.F. Lin, D.S. Chuu, K.W.-K. Shung, Phys. Rev. B 56 (1997) 1430.
[38] H. Ehrenreich, M.H. Cohen, Phys. Rev. 115 (1959) 786.
[39] T. Ando, J. Phys. Soc. Jpn. 74 (2005) 777.
[40] X. Blase, L.X. Benedict, E.L. Shirley, S.G. Louie, Phys. Rev. Lett. 72 (1994) 1878.
[41] K. Kempa, Phys. Rev. B 66 (2002) 195406.
[42] W. Vogel, D.-G. Welsch, Quantum Optics, Wiley-VCH, NY, 2006. p. 337 (Chapter 10).
[43] E. Hanamura, Phys. Rev. B 38 (1998) 1228.
[44] J.P. Reithmaier, G. Sęk, A. Löffler, C. Hofmann, S. Kuhn, S. Reitzenstein, L.V. Keldysh, V.D. Kulakovskii, T.L. Reinecke, A. Forchel, Nature 432 (2004) 197.
[45] T. Yoshie, A. Scherer, J. Hendrickson, G. Khitrova, H.M. Gibbs, G. Rupper, C. Ell, O.B. Shchekin, D.G. Deppe, Nature 432 (2004) 200.
[46] E. Peter, P. Senellart, D. Martrou, A. Lemaître, J. Hours, J.M. Gérard, J. Bloch, Phys. Rev. Lett. 95 (2005) 067401.
[47] D.A.B. Miller, D.S. Chemla, T.C. Damen, A.C. Gossard, W. Wiegmann, T.H. Wood, C.A. Burrus, Phys. Rev. Lett. 53 (1984) 2173.
[48] D.A.B. Miller, D.S. Chemla, T.C. Damen, A.C. Gossard, W. Wiegmann, T.H. Wood, C.A. Burrus, Phys. Rev. B 32 (1985) 1043.
[49] A. Zrenner, E. Beham, S. Stufler, F. Findeis, M. Bichler, G. Abstreiter, Nature 418 (2002) 612.
[50] H.J. Krenner, E.C. Clark, T. Nakaoka, M. Bichler, C. Scheurer, G. Abstreiter, J.J. Finley, Phys. Rev. Lett. 97 (2006) 076403.